FANKUCHEN, I. (1949). Private communication quoted by Lipscomb (1949).
HART, M. & LANG, A. R. (1961). *Phys. Rev. Lett.* **7**, 120–122.
KAMBE, K. (1957). *J. Phys. Soc. Jpn*, **12**, 13–31.
LAUE, M. VON (1931). *Ergeb. Exakten Naturwiss.* **10**, 133–158.
LIPSCOMB, W. N. (1949). *Acta Cryst.* **2**, 193–194.
MADSEN, J. U. & COTTERILL, R. M. J. (1978). *Acta Cryst.* A**34**, 378–384.
MAIN, P., WOOLFSON, M. M., LESSINGER, L., GERMAIN, G. & DECLERCQ, J. P. (1974). *MULTAN* 74. *A Computer Program for the Automatic Solution of Crystal Structures*. Univs. of York, England & Louvain, Belgium.
MIYAKE, S. & KAMBE, K. (1954). *Acta Cryst.* **7**, 218–220.
MOON, R. M. & SHULL, C. G. (1964). *Acta Cryst.* **17**, 805–812.
POST, B. (1977). *Phys. Rev. Lett.* **39**, 760–763.
RENNINGER, M. (1937). *Z. Phys.* **106**, 141–176.
WAGNER, E. (1920). *Phys. Z.* **21**, 632.

Acta Cryst. (1982). A**38**, 417–425

Coordinated Use of Isomorphous Replacement and Layer-Line Splitting in the Phasing of Fiber Diffraction Data

BY GERALD STUBBS

Rosenstiel Center, Brandeis University, Waltham, MA 02254, *USA*

AND LEE MAKOWSKI

Department of Biochemistry, College of Physicians and Surgeons of Columbia University, 630 *West* 168*th Street, New York, NY* 10032, *USA*

(*Received* 14 *September* 1981; *accepted* 18 *January* 1982)

Abstract

In order to calculate electron density maps from fiber diffraction patterns, the terms which superimpose because of cylindrical averaging of the pattern must be separated and their phases determined. This can be done using a technique analogous to the isomorphous replacement method of protein crystallography, but large numbers of heavy-atom derivatives are required. Because of the cylindrical averaging, the number of derivatives increases with increasing resolution. This paper describes a method for measuring the fine splitting of layer lines which occurs when a helical structure repeats approximately, but not exactly, in a given number of turns, and for using this as a source of phase information. The amount of phase information obtainable from each heavy-atom derivative is theoretically doubled since differences in both layer-line intensity and apparent layer-line position can be used, and this substantially increases the resolution attainable with a limited number of derivatives. The method is used to calculate an electron density map of tobacco mosaic virus at 6·7 Å resolution using only two derivatives instead of the four which would have been required using previously available methods.

Introduction

Structure determination using fiber diffraction is complicated by the fact that fiber diffraction data are cylindrically averaged. This is because the particles (such as rod-shaped viruses or helical nucleic acid molecules) that make up a fiber diffraction specimen are randomly oriented about their long axes. Model building, that is, the construction of models and the refinement of their parameters against the observed data, has been an effective way of determining structures such as nucleic acids and polysaccharides, but the great complexity of the macromolecular subunits in such sytems as helical viruses and rod-shaped intracellular assemblies limits the value of this approach. Stubbs & Diamond (1975) showed that the information lost by cylindrical averaging can be recovered by a technique analogous to the isomorphous replacement method of protein crystallography, but this method requires the preparation of a large number of heavy-atom derivatives. For example, to solve the structure of tobacco mosaic virus (TMV) at a resolution of 4 Å, six derivatives were required (Stubbs, Warren & Holmes, 1977). The number of derivatives increases with resolution, and at 3 Å

0567-7394/82/040417-09$01.00

resolution eight or more would be needed. These requirements for large numbers of heavy-atom derivatives limit the resolution to which isomorphous replacement can be used in the analysis of fiber diffraction data.

Diffraction from particles periodic in one dimension is limited to discrete layer planes in reciprocal space, which give rise to the observed layer lines (see Fig. 1 for an example). The spacing of the layer lines is reciprocal to the axial repeat distance of the particles in the specimen. Intensity on a layer line is made up of Bessel function terms, each of which is related to a cylindrical harmonic of the scattering particle. The contribution to the observed intensity from each Bessel function term must be determined in order to obtain the structure of the scattering units.

In many cases, the Bessel function terms contributing to a layer line do not fall at exactly the same distance from the equator; that is, the intensity on the layer line is split (Franklin & Klug, 1955). This occurs when the apparent repeat distance of the scattering particles (reflected in the layer-line spacing) corresponds only to an approximate repeat, the exact repeat distance being much longer. The degree of splitting is determined by the degree of deviation from an exact repeat, or, equivalently, by the length of the exact axial repeat. This splitting, if it can be measured, provides an opportunity for separating the contributions from Bessel functions superimposed on a layer line. In practice, splitting as such is not directly observed, because imperfect orientation of the particles in the specimen causes the diffracted intensity to be spread along Debye–Scherrer arcs. The effect of layer-line splitting, when the degree of splitting is small compared to the magnitude of the disorientation, is to cause shifts in the apparent position of the layer line which depend on the relative magnitudes of the contributing Bessel-function terms. Fig. 1 shows this effect in TMV. Preliminary studies (Makowski, 1980) have shown that these apparent shifts in layer-line positions can be measured by an elaboration of angular deconvolution (Makowski, 1978) and used to determine the contributions from two Bessel-function terms superimposed on a layer line.

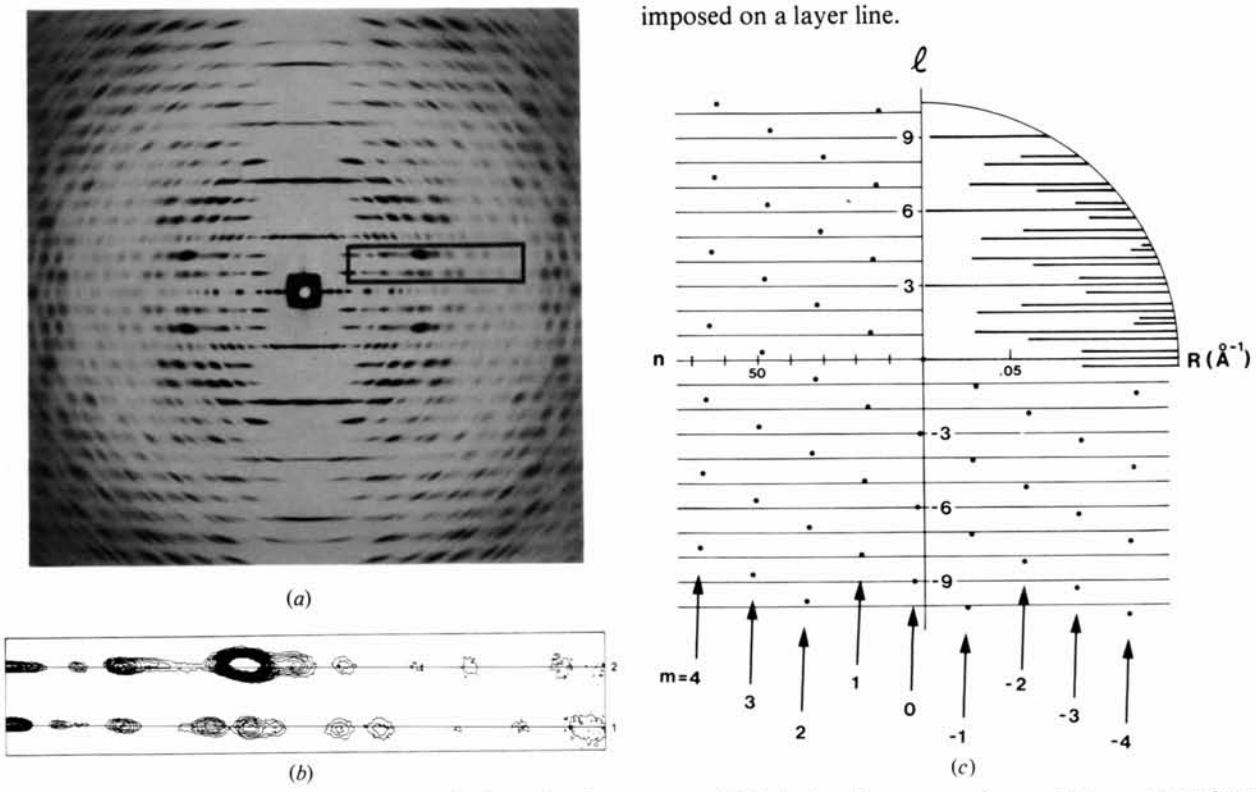

Fig. 1. (*a*) Diffraction pattern from tobacco mosaic virus, taken in an evacuated Guinier focusing camera using a point-focused beam from two bent quartz monochromators. (*b*) Contour map of the optical density in the part of (*a*) inside the box. The straight lines indicate the positions of layer lines 1 and 2 based on their positions near the meridian. It is evident that several of the intensity peaks are significantly off these lines. (*c*) Positions of the (n,l) terms of the TMV diffraction pattern, predicted on the basis of $49 + x$ subunits in three turns. An exaggerated value of $x = 0{\cdot}1$ has been used for clarity in the drawing. In reality, the terms on a given layer line are much closer together than this. [For TMV as shown in (*a*), $x = 0{\cdot}019$.] In the left and lower right quadrants, dots indicate values of n and their corresponding l_m [the (n,l) plot]. The upper right quadrant indicates the actual terms in the pattern, obtained by imposing *mm* symmetry on the (n,l) plot and replacing the dots with lines representing Bessel-function terms. These include high-order terms which were not included in the analysis in this paper. These terms come only from the outer part of the TMV particle at this resolution, and make only a small contribution to the intensity. This figure is similar to Fig. 1(*b*) of Franklin & Klug (1955).

In this paper we show that it is possible to measure the small differences in layer-line shifts between native TMV and heavy-atom derivatives, and that these differences provide independent information which can be used in structure determination. Isomorphous replacement and layer-line splitting are combined to determine the structure of TMV at 6·7 Å resolution using only two heavy-atom derivatives, rather than the four which would have been required using previously available methods.

Theory

1. *Diffraction from helical structures*

In diffraction from helical structures, electron density (ρ) is usually calculated in cylindrical coordinates r, φ and z. It is obtained from a set of complex Fourier–Bessel structure factors **G** by the relationships (Klug, Crick & Wyckoff, 1958)

$$\rho(r,\varphi,z)=\frac{1}{c}\sum_{l=-\infty}^{\infty}\sum_{n=-\infty}^{\infty}\mathbf{g}_{n,l}(r)\exp\left[i\left(n\varphi-\frac{2\pi lz}{c}\right)\right] \quad (1)$$

and

$$\mathbf{g}_{n,l}(r)=\int_0^{\infty}\mathbf{G}_{n,l}(R)J_n(2\pi Rr)2\pi R\,dR, \quad (2)$$

where R is reciprocal-space radius, l is the layer-line number, c is the repeat distance along the helix axis, and n is the order of the Bessel function J_n. The contribution to the electron density from each term $\mathbf{g}_{n,l}(r)$ in (1) is the projection of the electron density along a helix of pitch nc/l.

In the diffracting systems being considered here, the particles, although nearly parallel, are randomly oriented about their helical axes, so the diffracted intensity is cylindrically averaged in reciprocal space. Under these conditions, Waser (1955) and Franklin & Klug (1955) showed that the observed intensity I is

$$I(R,l)=\sum_n \mathbf{G}_{n,l}(R)\mathbf{G}^*_{n,l}(R). \quad (3)$$

If the diffracting helical structure has u identical subunits in t turns of the helix, where u and t are integers, the terms contributing to the sums in (1) and (3) are restricted to values of n and l which satisfy the selection rule

$$l=tn+um,$$

where m is integral (Cochran, Crick & Vand, 1952). If there is an almost, but not exactly, integral number of subunits $u+x(|x|\ll 1)$ in t turns, layer line l will be split, with the (n,l) term falling at $l_m=l+xm$ rather than exactly on l. For example, TMV (Fig. 1) has 49·019 subunits in three turns (see below). The $\mathbf{G}_{-16,1}$ term falls at $l_m=1{\cdot}019$. The **G** terms do not interfere with each other whether or not they fall exactly on the layer line, so (3) still holds.

2. *Isomorphous replacement*

To calculate an electron density map using (1) and (2), it is necessary to determine the real and imaginary parts of each **G** term contributing to the intensity in (3). In practice, the selection rule and the fact that Bessel functions have insignificant values until the argument approximates the order ensure that there will be a small number of terms in (3), the number increasing with the resolution of the intensity data. These terms may be separated using data from isomorphous heavy-atom derivatives (Stubbs & Diamond, 1975).

If $A_{j,i}$ represents a real *or* imaginary contribution to $\mathbf{G}_j$, where j indicates a particular data set, (3) may be rewritten for the native structure:

$$I_0=\sum_i A_{0,i}^2. \quad (4)$$

The subscript 0 denotes the native. If, in heavy-atom derivative j, the heavy-atom contribution at the reciprocal-space point under consideration is $a_{j,i}$ then the derivative intensity I_j is

$$I_j=\sum_i (A_{0,i}+a_{j,i})^2. \quad (5)$$

We combine (4) and (5) to obtain a linear equation in the unknowns $\{A_{0,i}\}$:

$$\sum_i a_{j,i}A_{0,i}=\tfrac{1}{2}\left(I_j-I_0-\sum a_{j,i}^2\right). \quad (6)$$

Stubbs & Diamond (1975) showed how a set of linear equations such as (6), one from each heavy-atom derivative, could be solved, subject to (4) as a constraint, to obtain the parts of $\{\mathbf{G}\}$ necessary to calculate an electron density map. Two derivatives are needed for each **G** term.

3. *Layer-line splitting*

Further information about the relative sizes of the **G** terms and their phases is available from the splitting of the layer lines caused by the non-integral number of subunits in the approximate helical repeat distance. This information may be combined with isomorphous replacement information in the following way.

Because of specimen disorientation, the various **G** terms contributing to a layer line will overlap, even when the layer line is split. For example, in TMV on layer line 1 at $R=0{\cdot}2$ Å^{-1}, there are three terms, falling at layer line positions corresponding to $l_m=$

1·02, 0·96 and 1·08. Adjacent terms are separated along the Debye–Scherrer arc by 0·25°. However, the disorientation in a TMV specimen is over 1°, so only a single peak is observed. If the splitting is much smaller than the disorientation, as is the case in TMV, the angular profile of the layer line will still be approximately Gaussian. The position of the center of this Gaussian will depend on the relative contributions of the **G** terms. If the fractional contribution from $A^2_{0,i}$ is h_i (that is, $h_i = A^2_{0,i}/I_0$), the arc will appear to be a Gaussian with its center displaced from the expected position by an angle Φ, where

$$\Phi = \sum \varphi_i h_i. \tag{7}$$

φ_i is the difference between the angular position of the center of the arc from $\mathbf{G}_i$, and the angular position φ_l that the layer line would have if there were no splitting. Multiplying (7) by I_0, we obtain for the native

$$\Phi_0 I_0 = \sum_i \varphi_i A^2_{0,i}. \tag{8}$$

This is a parallel equation to (4).*

The observed layer-line position for derivative j, Φ_j, will in general not be equal to the observed layer-line position in the native, Φ_0. The small differences between Φ_0 and Φ_j (see Fig. 2 for an example) can be used as a further, independent source of phase information. We can write, parallel to (5) and (8),

$$\Phi_j I_j = \sum_i \varphi_i (A_{0,i} + a_{j,i})^2 \tag{9}$$

and, parallel to (6),

$$\sum_i \varphi_i a_{j,i} A_{0,i} = \tfrac{1}{2}\left(\Phi_j I_j - \Phi_0 I_0 - \sum_i a^2_{j,i}\right). \tag{10}$$

These relationships assumed that the helical symmetry of the heavy-atom derivatives is exactly the same as the native helical symmetry. However, in TMV, an increase in the azimuthal separation of adjacent subunits of as little as 0·01 Å at the outside of the particle would double the observed splitting. Thus it is reasonable to assume, and observations have confirmed, that some changes in layer-line splitting will be observed among the derivatives. Setting the ratio of the degree of splitting in the jth derivative to that in the native equal to q_j, the position of the term $\mathbf{G}_i$ in the derivative will be equal to $q_j \varphi_i$. Then (9) becomes

$$\Phi_j I_j = \sum_i q_j \varphi_i (A_{0,i} + a_{j,i})^2 \tag{11}$$

and (10) becomes

$$\sum_i \varphi_i a_{j,i} A_{0,i} = \tfrac{1}{2}\left(\frac{\Phi_j}{q_j} I_j - \Phi_0 I_0 - \sum_i \varphi_i a^2_{j,i}\right). \tag{12}$$

Equation (12) represents a set of linear equations which can be combined with (6) in the calculation of phases. Furthermore, (8) is an independent source of phase information. Thus, if we have a native and n heavy-atom derivatives, of which m are sufficiently well oriented to give accurate measurements of splitting, we have at our disposal $n + m$ independent linear equations [n in the form of (6) and m in the form of (12)], and two quadratic equations [(4) and (8)]. The use of these equations will be discussed in the next section.

* We assume, both here and in (4), that $A(R, l)$ does not change significantly with the change in R along the arc from one **G** to another: that is, that all terms in (4) and (8) refer to the same R. Because disorientation spreads data out along arcs centered at the origin, on a layer line with two Bessel-function terms, the contribution at R from the term closer to the equator will overlap the intensity due to the second term at $R - \Delta R$, slightly closer to the meridian. $\Delta R \simeq (xm/c) \tan \varphi_l$. This is extremely small except near the meridian where $\varphi_l \to 90°$. However, near the meridian only one Bessel-function term contributes. Thus the effect is unimportant.

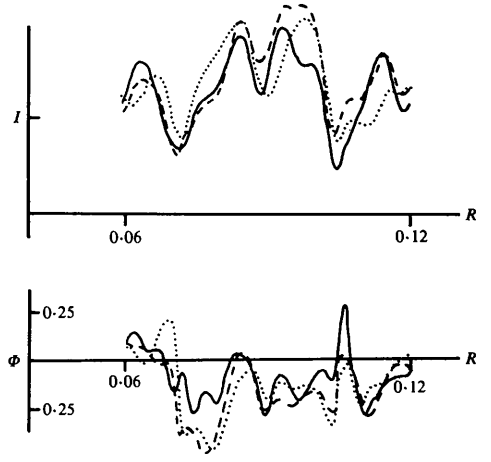

Fig. 2. Plots of intensity (I) and angular position (Φ) on layer line 1 as functions of reciprocal-space radius R. Solid lines: TMV. Broken lines: TMV–MMN. Dotted lines: Ni–2068–MMN.

4. *Angular deconvolution*

In order to use the theory given above to separate Bessel-function terms, it is necessary to measure both intensities and layer-line positions very accurately. This is done using a numerical deconvolution procedure (Makowski, 1978). The form of the optical density, $D(r, \varphi)$, in a fiber diffraction pattern can be expressed as a sum of contributions from the intensity on each layer line l contributing at that radius, $I_l(r, \varphi_l)$, plus the background, $B(r, \varphi)$:

$$D(r, \varphi) = \sum_l I_l(r, \varphi_l) f(\varphi - \varphi_l) + B(r, \varphi), \tag{13}$$

where r is the distance from the center of the diffraction pattern and φ is the angle about the center of the

diffraction pattern measured from the equator. The angular intensity distribution function, $f(\varphi - \varphi_l)$, describes the spreading out of the intensity as a function of angle φ. This angular smearing causes a reflection centered at (r, φ_l) to contribute to the optical density at (r, φ). For a Gaussian distribution of particle orientations, Holmes & Barrington Leigh (1974) showed that the angular intensity distribution function was approximately a Gaussian, and this is an adequate assumption for the data analyzed here. The background can usually be expressed as a sum of one or a few simple analytical functions of angle; for instance, the background can be expanded as a sum of orthogonal functions such as a Fourier series. One to three background terms have usually been utilized, the first term always being a circularly symmetric component.

With these assumptions, (13) becomes

$$D(r,\varphi) = \sum_{l=1}^{n_a} I_l(r,\varphi_l) \exp[-(\varphi - \varphi_l)^2/2\sigma^2] + \sum_{k=1}^{n_b} B_k(r) b_k(\varphi), \quad (14)$$

where σ is the standard deviation of the disorientation of particles in the specimen and the $b_k(\varphi)$ are the analytical functions of the background expansion. The $I_l(r,\varphi_l)$ and the $B_k(r)$ are the unknowns to be solved for at each radius r, where there are n_a unknown intensities and n_b unknown background parameters. The intensities, $I_l(r,\varphi_l)$, are equal to the background-subtracted optical densities at the centers of the layer lines.

Assuming that all the positions (r, φ_l) are known for all layer lines contributing at a radius r, the intensities and background parameters can be determined by measuring $D(r,\varphi)$ at a number of positions φ, and solving the set of equations (14). However, when layer-line splitting is present, the observed angular positions, Φ, of a layer line need not correspond to the expected value φ_l. On a layer line where splitting is present, the Bessel-function terms are not exactly superimposed, and the apparent position of the center of the layer line will depend on the relative intensities of the Bessel-function terms as given in (7). Accordingly, angular deconvolution was carried out to determine both the layer-line intensities, $I_l(r,\varphi_l)$ and the angular positions, Φ, as follows: Since the φ_l are known approximately, the linear equations (14) were solved assuming no layer-line splitting. Then, for each reflection, a limited, one-dimensional search was made for a position which better fit the measured intensities. The angular standard deviations, σ, were also allowed to vary since splitting leads to an apparent increase in the measured angular widths of the layer lines. Once a new set of positions and widths was determined, the set of linear equations was solved a second time. The cycle was repeated, if necessary, until no substantial changes were found in I or Φ. At the resolution of this work, one cycle was usually adequate, but at 4 Å resolution and beyond, up to three cycles have been required.

We note that in principle σ could be used as a source of phase information. However, the variation in σ is smaller and is less directly related to the relative strength of the Bessel-function terms.

Methods

The major steps in the analysis of diffraction patterns included determination of intensities and layer-line positions by angular deconvolution, determination of the splitting parameters φ_i for all Bessel-function terms and q_j for all derivatives, and application of the phase equations (4), (6), (8) and (12).

1. *Determination of intensities and positions*

The data analyzed in the *Results* section were collected on cylindrical films with a Guinier camera, of diameter 11·2 cm (Holmes, Stubbs, Mandelkow & Gallwitz, 1975). The films were measured with an Optronics Photoscan densitometer, using a 50 μm raster. The resulting computer images were used to obtain images in polar coordinates, having a radial grid spacing of 50 μm and an azimuthal spacing of 1°. For computational convenience, these were projected onto positions on a flat film by a simple geometric transformation (Fraser, Macrae, Miller & Rowlands, 1976). Angular deconvolution then provided the required intensities and layer-line positions. The intensities were corrected for non-linearity of film response, polarization and geometric effects.

2. *Determination of splitting parameters*

In order to use (8) and (12) in the solution of the phase problem, the parameters φ_i and q_j must be evaluated. q_j is simply the ratio of φ_i for a derivative to φ_i for the native. φ_i, the angular distance of a Bessel-order term from the predicted position of the unsplit layer line, is related to x, where there are $u + x$ subunits in t terms, by the equation

$$\varphi_i = xm/Rc.$$

Where only one Bessel order contributes to the diffraction pattern, for example layer lines 1 and 2 for $R < 0{\cdot}06$ Å^{-1}, $\varphi_i = \Phi$, the observed angular displacement. In these cases, x (calculated from Φ) was plotted as a function of R, and an average value of x was determined from the region where x was observed to be a constant. Fig. 3 shows these plots for native TMV. In this case, the observed layer lines are at $l_{obs} = 1{\cdot}019$ and $l_{obs} = 1{\cdot}981$. Thus, $x = 0{\cdot}019$. It should be noted that although x varies between the native and

Table 1. *Number of subunits in three turns of the helix ($u + x$, where $u = 49$) and ratio (q) of x to the value of x found for native TMV, for the various heavy-atom derivatives of TMV used by Stubbs, Warren & Holmes* (1977)

Derivative	$u + x$	q
Native	49·019	(1·0)
TMV–MMN	49·024	1·3
Ni–2068–MMN	49·022	1·2
TMV–Os	49·022	1·2
TMV–SHIMS–MMN	49·033	1·7
TMV–Pb	49·022	1·2
TMV–UF	49·019	1·0

derivatives (that is, $q_i \neq 1{\cdot}0$), the variation is not sufficient to indicate serious non-isomorphism. The largest value of q which we have observed, 1·7 (see Table 1), represents a change in the azimuthal separation of adjacent subunits at the outside of the particle of only 0·01 Å.

This method allows very precise determination of the splitting parameters, particularly if, as was usually the case in this work, Φ as a function of R is first smoothed by eliminating high-frequency variations. Agreement between values determined from different layer lines has always been excellent up to at least layer line 5. Table 1 gives helical parameters and values of q for all the derivatives used by Stubbs, Warren & Holmes (1977).

Note on smoothing: Since no squared Bessel-function term can fluctuate with a frequency higher than $2a$, where a is the radius of the TMV particle, ΦI, which is a linear combination of such terms [equation (8)], can have no higher-frequency components than this. Therefore, when required, smoothing was applied by computing the one-dimensional Fourier transform of $\Phi I(R)$, omitting the high-frequency terms and back-transforming before dividing by $I(R)$. The high-frequency cut was applied at the first node in the transform after $2a$.

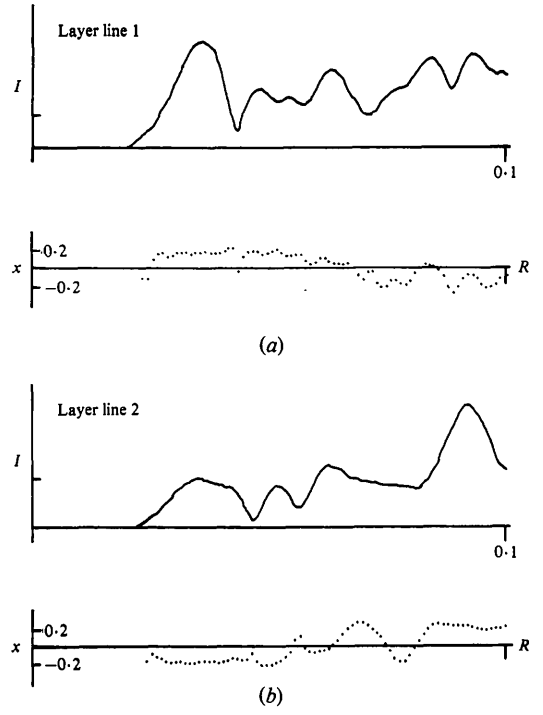

Fig. 3. Plots of intensity (I) and x (calculated from Φ) as functions of reciprocal-space radius R. The calculation of x is only valid at low values of R, for which only one Bessel-function term contributes to the intensity. For these values, x is seen to be approximately constant. There are $49 + x$ subunits in three turns of TMV. Units of I are arbitrary. Units of R are Å^{-1}.

3. *Determination of phases and Bessel-order separation*

With data sets from a native and sufficient heavy-atom derivatives, known splitting parameters and known heavy-atom positions (see Stubbs, Warren & Holmes (1977) for references on locating heavy atoms), it is possible to use equations (4), (6), (8) and (12) to determine the real and imaginary parts of all the **G** terms contributing to a point (R,l). The procedure used in this work was to use the linear equations (6) and (12) to obtain a preliminary solution by a linear least-squares procedure, and to take this solution as a starting point for a non-linear least-squares procedure which included (4) and (8).

The relative weighting of the equations is an important consideration, since they involve parameters of dramatically different magnitudes. We used weights based on the expected errors in the equations in the usual way (Topping, 1955); but rather than attempt a detailed error analysis (which would be complicated by the difficulty of estimating errors in the non-linear angular deconvolution), we made rough estimates for each type of equation. For example, if the error ε_{I_0} in (4) is normalized to 1, we estimate the error in (8) from the formula $\varepsilon = (I_0^2\,\varepsilon_{\Phi_0}^2 + \Phi_0^2\,\varepsilon_{I_0})^{1/2}$ (Topping, 1955) to be typically 0·001. Similar formulae give for (6) $\varepsilon \simeq 1$, and for (12) $\varepsilon = 0{\cdot}001$. We have found that varying these estimates by a factor of two in either direction has no significant effect on our electron density maps.

Layer-line splitting is of no value in determining phases on the equator, since for every Bessel-function term $\mathbf{G}_n$ present with an expected position of φ, $\mathbf{G}_{-n}$ is present at $-\varphi$, so $\Phi \equiv 0$. However, the simple relationships between $\mathbf{G}_n$ and $\mathbf{G}_{-n}$ reduce the number of unknowns on the equator by almost half, so isomorphous replacement alone provides adequate phase information.

Results

The methods outlined above were applied to the solution of the structure of TMV at 6·7 Å resolution using two heavy-atom derivatives. This solution was compared with the solution at the same resolution using isomorphous replacement alone, with six derivatives.

The two derivatives of TMV used were the derivative with methyl mercury nitrate (MMN) and the derivative of the Ni-2068 strain with MMN described by Stubbs, Warren & Holmes (1977). The films of Stubbs, Warren & Holmes were densitometered and processed by angular deconvolution as described under *Methods*. Intensity data and smoothed splitting data for a typical region of layer line 1 are shown in Fig. 2. Values of q were determined using smoothed splitting data from layer lines 1, 2, 4 and 5, and found to be 1·3 for TMV–MMN and 1·2 for Ni–2068–MMN (Table 1).

It was assumed that only two Bessel orders were present in the diffraction pattern at this resolution. This is the assumption made by Holmes, Stubbs, Mandelkow & Gallwitz (1975) in their 6·7 Å resolution isomorphous-replacement map of TMV. From the smoothed data and with the methods described above, Bessel orders were separated, phases determined and an electron density map calculated. (It is of interest to note that a map calculated using unsmoothed splitting data is very similar to this map.)

The principal features of the TMV protein structure are four approximately radial α-helices, called the left and right radial and the left and right slewed helices by Champness, Bloomer, Bricogne, Butler & Klug (1976). These features, as well as the RNA, are quite clear in our map, part of which is shown in Fig. 4(*a*). The sections in this figure have been chosen so that the left radial α-helix falls in the plane of the figure. Part of the right radial helix and two bases of the RNA are also visible. For comparison, Fig. 4(*b*) shows the same region of a map calculated using isomorphous replacement alone, with the data of Stubbs, Warren & Holmes truncated at 6·7 Å resolution. This map used six derivatives, but it is not significantly better than the two-derivative map in Fig. 4(*a*). In both maps the left radial helix is quite distinct and density corresponding to the two bases and the outer portion of the right radial helix can be identified. Where the two maps disagree, comparison with the higher-resolution (4 Å) map of Stubbs, Warren & Holmes (1977) does not favour one map or the other.

Without using the splitting data, two derivatives cannot be used to separate uniquely the contributing Bessel function terms. However, we must show that our map is better than maps obtained using other methods for treating two-derivative data.

There are two obvious approaches: We could truncate the data at a resolution where only one Bessel order contributes significantly to each layer line, or we

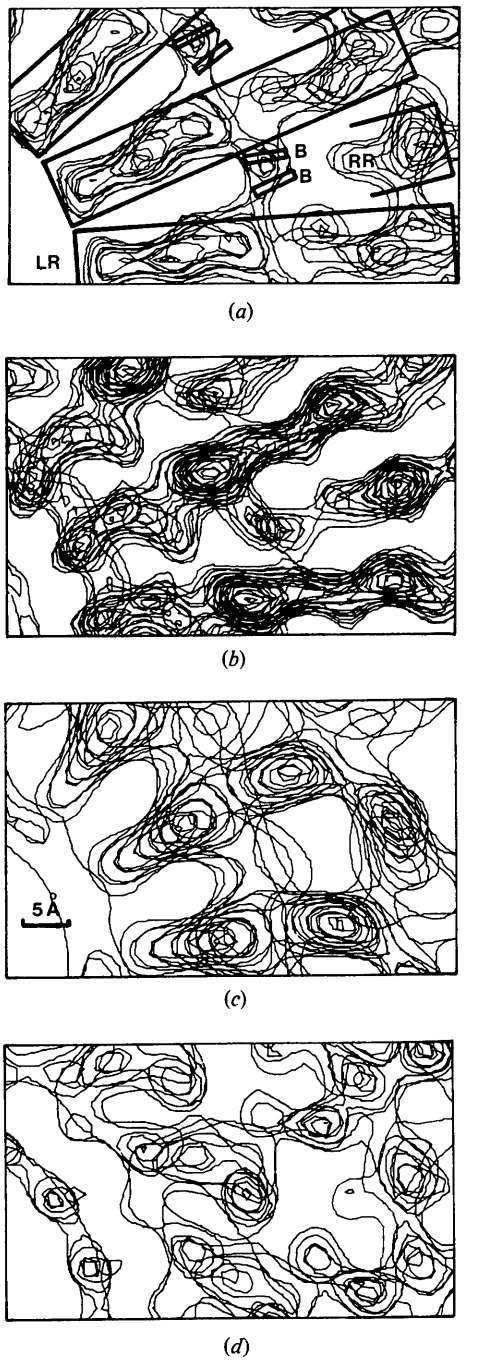

(*a*)

(*b*)

(*c*)

(*d*)

Fig. 4. Five superimposed sections, 1·4 Å apart, through part of the electron density map of TMV calculated in various ways. (*a*) Using layer-line splitting and isomorphous replacement with data from two derivatives. (*b*) Using isomorphous replacement alone from six derivatives. (*c*) Using isomorphous replacement alone from two derivatives; data truncated at 10 Å resolution. (*d*) Using isomorphous replacement data from two derivatives, and the arbitrary assumption that diffracted intensity is equally divided between the contributing Bessel-function terms. In (*a*), heavy outlines indicate the positions of the left radial α-helix (*LR*), part of the right radial helix (*RR*) and two RNA bases (*B*). Parts of three adjacent subunits are visible.

could make some arbitrary assumption about the relative intensities of the Bessel orders. The first approach is illustrated in Fig. 4(*c*), which was constructed using data truncated at 10 Å resolution. The one Bessel-function term contributing to each layer line was phased using the two derivatives. This is comparable to the procedure used by Barrett *et al.* (1971), and the map is similar to theirs. It is recognizably related to the higher-resolution maps, especially near the center of the virus, but it is clearly at a lower resolution. Arbitrary assumptions about the relative intensities of Bessel-function terms can be made in a variety of ways; for example we can choose to distribute the intensity randomly between two Bessel orders, assign all the intensity to the lower order, or divide the intensity equally between two Bessel orders (assigning all the intensity to one order at resolutions where the second order does not contribute). Equal division of the intensity between contributing Bessel function terms gave the best map of this type, which is shown in Fig. 4(*d*). However, although it shows considerable detail, the detail does not correspond to the known structure, and the map is actually inferior even to the 10 Å map.

The four maps are compared again in Fig. 5. In this figure, four sections perpendicular to the axis of the virus particle are superimposed to give a 4·2 Å thick section through two adjacent subunits at the level of the RNA. Parts of the RNA, the left and right radial helices and the 'hydrophobic girdle' [the concentration of aromatic groups at high radius identified by Bloomer, Champness, Bricogne, Staden & Klug (1978)] are clearly visible in the two-derivative splitting map (Fig. 5*a*) and the six-derivative isomorphous replacement map (Fig. 5*b*). The resolution of the 10 Å map (Fig. 5*c*) is too low to allow protein secondary structure units to be recognized, while the details of the map calculated by equal division of intensity (Fig. 5*d*) once again do not correspond to the known structure.

Conclusion

The structure of tobacco mosaic virus was first solved at 6·7 Å by Holmes *et al.* (1975) using multi-dimensional isomorphous replacement. That work required a minimum of four heavy-atom derivatives,

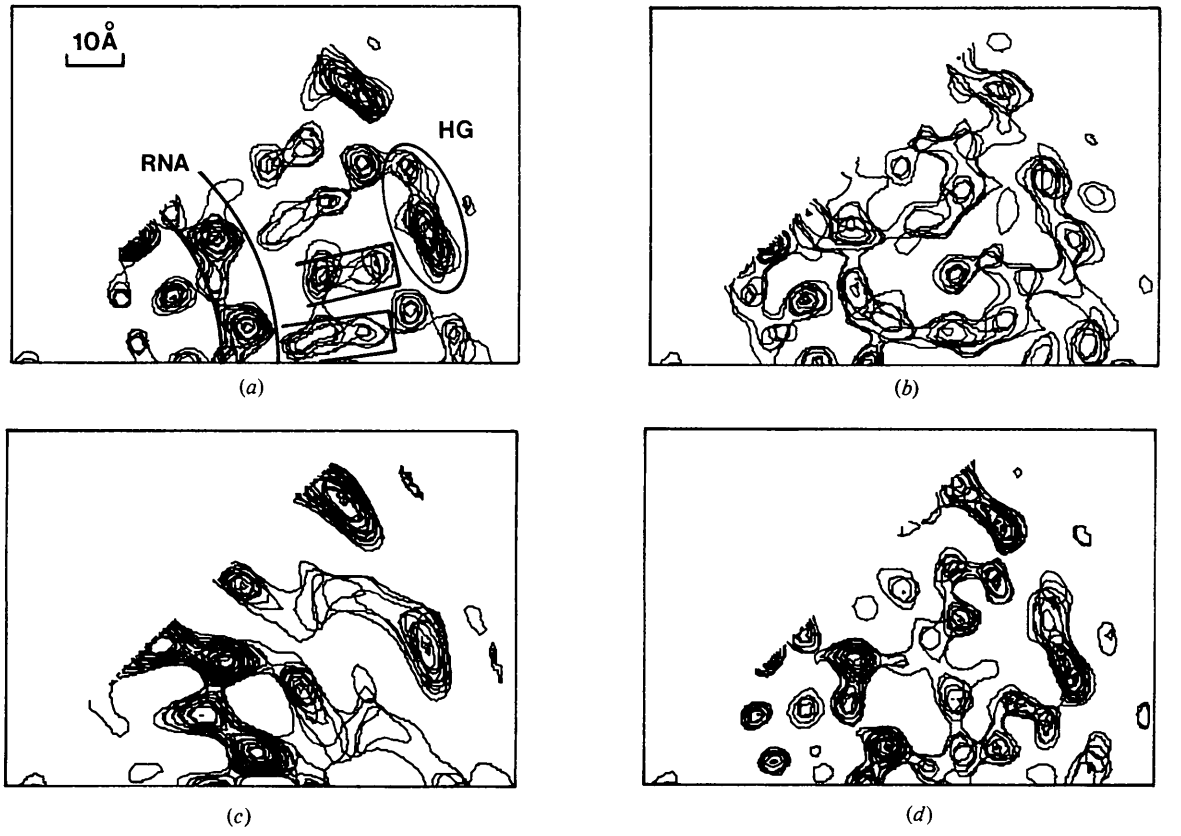

Fig. 5. Four superimposed sections, 1·4 Å apart, through part of the electron density map of TMV calculated in various ways. The methods of calculation used in (*a*) to (*d*) correspond to those in Fig. 4. Parts of the RNA and the 'hydrophobic girdle' (*HG*) are indicated in (*a*), as well as the left and right radial α-helices (open boxes).

and in fact used five. By utilizing the fine splitting of layer lines due to the imperfect repeat of the TMV helix (Makowski, 1980) and the small differences in splitting among the derivatives, we have solved the same structure using only two derivatives, obtaining an electron density map of comparable quality.

Structures other than TMV often have more Bessel orders contributing to a layer line at a given resolution, and use must be made of all available information to solve their structures. Preparation of heavy-atom derivatives for use in fiber diffraction is difficult, since most fiber structures are unusually sensitive to chemical disturbance [for example, microtubules (Ludueña, 1979)] or have surfaces with a specific protective function (as in viruses) and so are very resistant to modification. Furthermore, location of heavy atoms in a helical structure presents special difficulties (Holmes, Mandelkow & Barrington Leigh, 1972; Holmes *et al.*, 1975). Any method such as the one presented here which increases the information available from each derivative will greatly extend the resolution attainable in structural studies using fiber diffraction.

This work was supported by NIH grants GM25236, CA24407 and CA29522, and by an Alfred P. Sloan Foundation Fellowship to LM.

References

BARRETT, A. N., BARRINGTON LEIGH, J., HOLMES, K. C., LEBERMAN, R., MANDELKOW, E., VON SENGBUSCH, P. & KLUG, A. (1971). *Cold Spring Harbor Symp. Quant. Biol.* **36**, 433–448.

BLOOMER, A. C., CHAMPNESS, J. N., BRICOGNE, G., STADEN, R. & KLUG, A. (1978). *Nature (London)*, **276**, 362–368.

CHAMPNESS, J. N., BLOOMER, A. C., BRICOGNE, G., BUTLER, P. J. G. & KLUG, A. (1976). *Nature (London)*, **259**, 20–24.

COCHRAN, W., CRICK, F. H. C. & VAND, V. (1952). *Acta Cryst.* **5**, 581–586.

FRANKLIN, R. E. & KLUG, A. (1955). *Acta Cryst.* **8**, 777–780.

FRASER, R. D. B., MACRAE, T. P., MILLER, A. & ROWLANDS, R. J. (1976). *J. Appl. Cryst.* **9**, 81–94.

HOLMES, K. C. & BARRINGTON LEIGH, J. (1974). *Acta Cryst.* A**30**, 635–638.

HOLMES, K. C., MANDELKOW, E. & BARRINGTON LEIGH, J. (1972). *Naturwissenschaften*, **59**, 247–254.

HOLMES, K. C., STUBBS, G. J., MANDELKOW, E. & GALLWITZ, U. (1975). *Nature (London)*, **254**, 192–196.

KLUG, A., CRICK, F. H. C. & WYCKOFF, H. W. (1958). *Acta Cryst.* **11**, 199–213.

LUDUEÑA, R. F. (1979). *Microtubules*, edited by K. ROBERTS & J. S. HYAMS. New York: Academic Press.

MAKOWSKI, L. (1978). *J. Appl. Cryst.* **11**, 273–283.

MAKOWSKI, L. (1980). In *Fiber Diffraction Methods*, edited by A. D. FRENCH & K. H. GARDNER. American Chemical Society Symposium Series, Vol. 141, pp. 139–148.

STUBBS, G., WARREN, S. & HOLMES, K. (1977). *Nature (London)*, **267**, 216–221.

STUBBS, G. J. & DIAMOND, R. (1975). *Acta Cryst.* A**31**, 709–718.

TOPPING, J. (1955). *Errors of Observation and Their Treatment*. New York: Reinhold.

WASER, J. (1955). *Acta Cryst.* **8**, 142–150.

Acta Cryst. (1982). A**38**, 425–432

Bragg Diffraction From a Material of Circular Cross Section

BY D. K. SALDIN*

Department of Metallurgy and Science of Materials and Department of Engineering Science, University of Oxford, Oxford, England

(*Received* 10 *October* 1981; *accepted* 22 *January* 1982)

Abstract

The problem of dynamical Bragg diffraction from a set of Bragg planes in a material circular in the diffraction plane is solved by a combination of a Riemann-function technique and numerical integration of the Takagi–Taupin equations. In regions affected by non-Laue surfaces the solution is compared with an approximate Green-function method based on truncation of small arcs of the circle. The bright-field and dark-field intensity profiles are determined only by the radius of the circle compared to the extinction distance, and on the absorption parameters. The dependence of the profiles on these parameters is studied.

* Present address: Blackett Laboratory, Department of Physics, Imperial College of Science and Technology, Prince Consort Road, London SW7, England.

0567-7394/82/040425-08$01.00